IEEE Access
Multidisciplinary | Rapid Review | Open Access Journal

Received August 13, 2019, accepted September 3, 2019, date of publication September 11, 2019, date of current version October 4, 2019.

Digital Object Identifier 10.1109/ACCESS.2019.2940899

A Novel Heading Angle Estimation Methodology for Land Vehicles Based on Deep Learning and Enhanced Digital Map

QIMIN XU[1], XU LI[1], (Member, IEEE), ZHENGLIANG SUN[2], WEIMING HU[1], AND BIN CHANG[1]

[1]School of Instrument Science and Engineering, Southeast University, Nanjing 210096, China
[2]Traffic Management Research Institute, Ministry of Public Security, Wuxi 214151, China

Corresponding author: Xu Li (lixu.mail@163.com)

This work was supported in part by the National Key Research and Development Program of China under Grant 2018YFB1600803, in part by the National Natural Science Foundation of China under Grant 41904024, in part by the National Natural Science Foundation of China under Grant 61973079, in part by the Program for Special Talents in Six Major Fields of Jiangsu Province under Grant 2017 JXQC-003, and in part by the Fundamental Research Funds for the Central Universities under Grant 2242019K40037.

ABSTRACT In this paper, a novel heading angle estimation methodology for land vehicles using low-cost sensors is proposed by combining the advantages of deep learning and enhanced digital map. First, an intelligent perception model of heading-related information with hybrid structure is designed to estimate the angle difference between the vehicle driving direction and the road direction. The intelligent perception model comprises of a CNN based feature extraction model and a LS-SVM based nonlinear regression model. The extracted senior features are utilized as the input of LS-SVM to predict the angle difference between the vehicle driving direction and the road direction. Then, an enhanced digital map is established to provide the road direction through map matching. Finally, the heading angle of the vehicle is obtained by combining the angle difference and the road direction. In theory, the proposed heading angle estimation methodology is not affected by the complex urban environment and is immune to cumulative errors. To verify the feasibility and effectiveness of the proposed methodology, field experiments on different road types and with different driving maneuvers were performed. The experimental results indicate that the proposed methodology can achieve accurate heading angle estimation.

INDEX TERMS Enhanced digital map, heading angle, intelligent model, vehicle state estimation.

I. INTRODUCTION

Accurate vehicle motion parameters are the foundation of autonomous driving and driving assistance system [1], [2]. Among all the vehicle motion parameters, the heading angle is one of the most significant ones [3]. First of all, the heading angle errors seriously affect the accuracy of the vehicle positioning solution in a complex urban environment [4]. Since the vehicle position is one of the most required information for many applications, such as vehicle navigation [5], Location Based Service (LBS) [6], etc., the heading angle errors will indirectly affect the overall performance of these applications. Besides, due to the limitation of the degree of freedom, the vehicle cannot move in an arbitrary direction. Thus, the heading information is required to control the vehicle [7], or the vehicle cannot be controlled to reach the destination.

For land vehicles, the highly accurate heading angle can be acquired by using high-quality fiber-optic gyro [8]. However, the high cost and government regulations impede the commercial use of that sensor [9]. For mass-market application, the sensors/methods which can acquire the heading angle should meet the requirement of low cost. At present, the estimation methods of heading angle for civil land vehicles can be categorized as direct measuring method and yaw rate based method:

1) DIRECT MEASURING METHOD

The digital compass and two-antenna GNSS are two sensors typically used to measure the heading angle of a moving vehicle.

The associate editor coordinating the review of this manuscript and approving it for publication was Kathiravan Srinivasan.

The digital compass uses the magnetic sensor to obtain the heading information by measuring the Earth's Magnetic Field, so the heading angle measured by the digital compass is actually relative to the magnetic north [10], rather than the geographical north (the true north). Although some compensation can be used to correct the output of the digital compass, the magnetic sensor is easily affected by the distortion of the orientation due to magnetic interference that is very frequently found in the urban environment.

In recent years, the two-antenna GNSS provides a highly accurate solution for the vehicle heading angle measurement [11]. Through installing two GNSS antennas along the longitudinal axis on the roof of the vehicle, the heading angle with high precision can be achieved with an appropriate baseline (the distance between the two antennas). However, the performance is severely affected by the status of GNSS, which usually suffers from the signal block and fails in a complex urban environment. Thus, the accuracy and reliability of the heading angle measured by the two-antenna GNSS cannot be guaranteed.

2) YAW RATE BASED METHOD

The yaw rate is the vehicle's angular velocity around its vertical axis. When the initial heading information of the vehicle is known, the vehicle heading angle at each moment can be obtained by integrating the yaw rate continuously [12]. The yaw rate estimation methods can be divided into four categories: gyro based [3], kinematics model based [13], dynamic model based [14], and machine vision based methods [15], [16]. Subject to the low-cost requirements of in-vehicle sensors and the vibration of in-vehicle environment, it is difficult to obtain highly accurate yaw rate and the estimated yaw rate usually contain some inevitable errors [17]. Considering the principle of the yaw rate based method, the heading angle is calculated through integration so that the accumulated errors cannot be avoided. Thus, the accuracy of heading angle estimation using this kind of method will decline over time.

For the methods mentioned above, it can be concluded that existing heading angle estimation methods are adversely affected by the complex operating environment or cumulative errors. In order to address these shortcomings, this paper proposes a novel heading angle estimation method for vehicles, which integrates the advantages of deep learning and enhanced digital map.

Deep learning, especially Convolutional Neural Networks (CNN), can grasp the high-level abstraction of raw image data [18]. CNN integrates the learning of target pattern features into the process of model establishment, and thus reducing the incompleteness of general machine learning algorithms caused by manual intervention in the feature extraction process [19]. At present, in the application of image classification and object detection, deep learning has been confirmed to be superior to traditional algorithms and can even surpass the average cognitive performance of human beings [20]. There is an increasing trend to apply deep learning to more research fields, including vehicle positioning, driving assistance, and autonomous driving.

With the popularization of the vehicle navigation system, there is an increasing requirement of the digital map. In recent years, the enhanced digital map has been developed by adding the road and traffic information to the traditional digital maps [21], [22]. Therefore, the function of the digital map has been expanded, more than just navigation. Usually, the road and traffic information contains traffic signs, traffic lights, number of lanes, lane width, road slope, road curvature, etc. The added information can be easily extracted by map matching.

In this paper, the proposed heading angle estimation methodology first estimates the angle difference between the vehicle driving direction and the road direction based on deep learning and then utilizes enhanced digital map to acquire the current road direction. Therefore, the vehicle heading angle can be obtained by combining the angle difference and the road direction. The main contributions of the paper can be summarized as:

1) An intelligent perception model of heading-related information with hybrid structure is proposed to estimate the angle difference between the vehicle driving direction and the road direction. The senior features are extracted based on CNN and then used for SVM regression. Experimental results indicate that the intelligent perception model can adapt to different motion types, including straight, curve and 90° turn. To the authors' knowledge, this aspect is seldom evaluated and discussed in the existing literature.

2) The proposed vehicle heading angle estimation methodology is not affected by the signal blockage in a complex urban environment or the cumulative errors in theory. Besides, since the main information required by the proposed solution comes from the camera and the enhanced digital map, the hardware cost can be maintained at a low level.

This paper is organized as follows. In the next section, the overview of the proposed heading angle estimation methodology is given. Section III explains the detailed implementation of the intelligent perception model of heading-related information. Section IV describes the design of the enhanced digital map containing road direction information. Section V presents the results of experimental validation. Section VI is the concluding remark.

II. OVERVIEW OF THE PROPOSED METHODOLOGY

In this paper, the deep learning and enhanced digital map are utilized to propose an intelligent vehicle heading angle estimation methodology. The mechanism and functionality are illustrated in Figure 1.

At first, the intelligent perception model of heading-related information is established based on deep learning. The angle difference between the current vehicle driving direction and the road direction is estimated by the input of the image taken by the forward-looking camera installed on the vehicle.

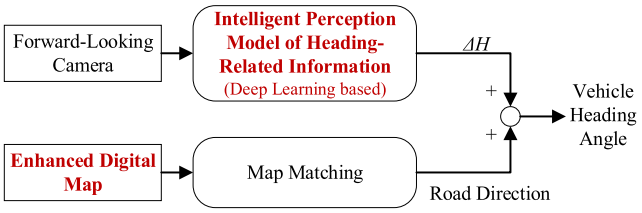

ΔH: the angle difference between vehicle driving direction and road direction

FIGURE 1. Diagram of the proposed novel heading angle estimation methodology.

Then, the enhanced digital map expands the road direction information on the basis of the traditional digital map, and the current road direction can be acquired by map matching. Through combining the current road direction and the angle difference between the current vehicle driving direction and the road direction, the current heading angle of the vehicle can be obtained.

There is no iterative process during the heading angle estimation using the proposed methodology, so the results are not affected by cumulative errors. When the training samples for the intelligent perception model of heading-related information are sufficient, the proposed methodology can adapt to various motion types and different environment. Therefore, the proposed methodology is not easily affected by the complex urban environment. In addition, with the popularity of dashcam and driving assistance equipment, the visual sensor has almost become the standard configuration of civil vehicles. The camera is affordable and widely used. Moreover, because the enhanced digital map belongs to the software equipment, it does not increase the hardware cost. Therefore, the proposed methodology is low-cost and has the potential for mass-market application.

Based on the estimation process shown in Fig 1, the accuracy of the proposed methodology is mainly affected by the following three factors: 1) the accuracy of the map matching algorithm; 2) the accuracy of the heading-related information estimated by the intelligent perception model; 3) the accuracy of the road direction information in the enhanced digital map.

At present, there are many published research articles about the map matching algorithms and most of them can achieve good performance with accurate position information. Thus, this paper will not focus on research about the map matching algorithm. The research work of this paper will focus on establishing the intelligent perception model of heading-related information based on deep learning and the enhanced digital map containing road direction information. The intelligent perception model of heading-related information is established based on the deep learning algorithm. Due to the diversity and non-universality of deep learning structure, it is necessary to develop the model structure according to our special task. For the enhanced digital map, there is no open-source map providing the road direction or unified enhanced digital map-making method at present. Thus, the design of enhanced digital map should also be carried out according to the requirements of our proposed methodology.

III. INTELLIGENT PERCEPTION MODEL OF HEADING-RELATED INFORMATION

In order to estimate the heading-related information, i.e. the angle difference between vehicle driving direction and road direction (denoted as ΔH), an intelligent perception model which adopts a hybrid structure is proposed based on the advanced deep learning algorithm. First, a CNN based feature extraction model is developed to excavate the feature of the input image. Every different ΔH value can be regarded as one kind of feature. However, this will lead to a large number of defined features. In this paper, we merge a certain range of ΔH into one kind of **senior feature** to reduce the total number of the features. Thus, the ΔH is divided into different categories and the feature extraction procedure can be transferred to a classification procedure. Then, a nonlinear regression model is carried out to predict ΔH based on the senior features, i.e. the classification results of ΔH. Since the classification and prediction of ΔH based on deep learning are seldom discussed, we have carried on the design of the overall model structure according to the characteristics of the ΔH, as shown in Figure 2.

A. CNN BASED FEATURE EXTRACTION MODEL

CNN is a viable and effective alternative for feature extraction [19]. It can directly use image pixel information as the input and conduct high-level abstraction through convolution operation to realize image identification, classification, etc. At present, some CNN-based classification models have been published and widely tested, including VGG-16, ResNet50, InceptionV3, etc. These models all have strong feature extraction ability and can achieve high accuracy when conducting large-scale and multi-categories classification on ImageNet dataset [23]. In this paper, the classification task has fewer categories than the tasks of the widely used models mentioned above. The structure of these existing models is not so suitable for our task. Therefore, we design a specific feature extraction model with reference to the existing model rather than use them directly.

According to the actual driving situation, the range of ΔH is defined as $[-90°, 90°]$. When deciding the range of ΔH, a conventional and simple method is linear division, namely each category of senior feature has the same range of ΔH. Considering that ΔH is small in most normal driving cases and $-90°$ or $90°$ only appears in extreme circumstances in actual, the linear division may easily lead to the uneven distribution of samples. Thus, we use a nonlinear method to divide the range of ΔH for better features expression. The principle is that the range should be divided densely when ΔH is small and the range should be divided sparsely when

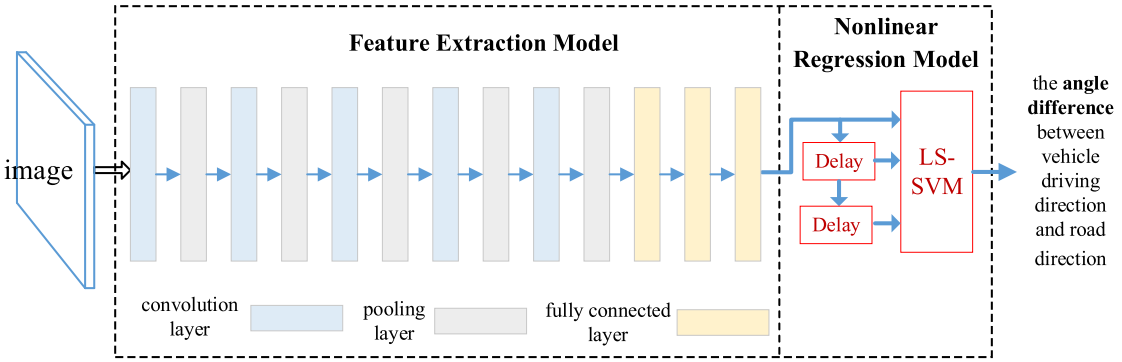

FIGURE 2. The hybrid structure of the intelligent perception model of heading-related information.

TABLE 1. Senior features labels and their corresponding ΔH range.

Label of the senior feature	Range of ΔH
0	[-90°,-64°]
1	[-64°,-49°]
2	[-49°,-36°]
3	[-36°,-25°]
4	[-25°,-16°]
5	[-16°,-10°]
6	[-10°,-6°]
7	[-6°,-3°]
8	[-3°,3°]
9	[3°,6°]
10	[6°,10°]
11	[10°,16°]
12	[16°,25°]
13	[25°,36°]
14	[36°,49°]
15	[49°,64°]
16	[64°,90°]

ΔH is large. Specifically, some actual driving experience is adopted to divide the range of $[-10°, 10°]$ to reliably distinguish the lane-changing maneuver, while other range is divided by using a square growth method. To balance the complexity of feature extraction model and the requirement to explicitly express the feature of ΔH, seventeen kinds of senior features are finally determined. For clarity, different numbers are used to represent different senior features. The senior features labels and their corresponding ΔH range are shown in Table 1.

The feature extraction model uses multi-layer CNN to extract the senior feature of the image. The multi-layer CNN architecture is based on the principle of the human visual system. Firstly, the basic object edges with directionality, such as horizontal, vertical and slant lines, are detected. Then, several edges are combined to represent the high-level features of some objects. Finally, the detected parts are comprehensively recognized and judged for different categories. Each deeper layer of CNN can extract more advanced features than the previous layer. Comprehensively considering the feature extraction ability and the complexity of the model, an eight-layer (five convolution layers and three fully connected layers) model structure is designed by referring to the VGG-16, as shown in Figure 2. Generally, CNN consists of three main layers: convolutional layer, pooling layer and fully connected layer [24].

The convolution layer uses the convolutional kernel to carry out convolution operation on the image matrix and then extracts image features through an activation function. We use the ReLu function as the activation function for the convolution layers.

The input image matrix is expressed as:

$$input = \begin{bmatrix} a_{11} & a_{12} & \cdots & a_{1H} \\ a_{21} & \ddots & \ddots & a_{2H} \\ \cdots & \ddots & \ddots & \cdots \\ a_{W1} & a_{W2} & \cdots & a_{WH} \end{bmatrix} \quad (1)$$

where a is the pixel information, W is the width of the image, and H is the height of the image.

This model adopts a small convolutional kernel of 3×3, which can reduce the number of parameters and keep the appropriate local receptive field [25]. The small convolutional kernel will contribute to the fast and effective feature extraction [26]. The expression of the convolutional kernel can be written as:

$$filter = \begin{bmatrix} h_{11} & h_{12} & h_{13} \\ h_{21} & h_{22} & h_{23} \\ h_{31} & h_{32} & h_{33} \end{bmatrix} \quad (2)$$

where h indicates the parameter of the convolutional kernel.

In the process of convolution operation, the convolutional kernel (filter) is used as a window and sweep over the input image matrix successively with a certain stride in the order of from left to right and from top to bottom. In order to ensure that the feature image obtained from the convolution operation has the same size as the original image, the zero-padding method is used to fill the edge pixel of the original image with the value of 0. The calculation method of convolution

operation is:

$$\begin{aligned} net_{oij} &= conv(input, filter) \\ &= a_{i,j} \times h_{11} + a_{i,j+1} \times h_{12} + a_{i,j+2} \times h_{13} + a_{i+1,j} \times h_{21} \\ &\quad + a_{i+1,j+1} \times h_{22} + a_{i+1,j+2} \times h_{23} + a_{i+2,j} \times h_{31} \\ &\quad + a_{i+2,j+1} \times h_{32} + a_{i+2,j+2} \times h_{33} \\ &\quad 1 \le i \le W,\ 1 \le j \le H \end{aligned} \quad (3)$$

The output of the convolution layer, i.e. the feature image, has a lot of redundant information. Thus, the pooling layer can be used to reduce the size of the feature image. The translation invariability of the pooling layer can retain the basic information of the feature image [27]. Similar to the convolution operation, the practice of pooling layer also uses a window to slide over the feature images after convolution to realize dimension reduction. The difference is that there is no overlap between each sliding window during pooling operation. This model adopts the max pooling method to achieve better feature extraction than the average pooling method [28]. When the size of the feature image is reduced by the execution of pooling layer, the model parameters are also reduced. Thus, the pooling layer can contribute to improving the real-time performance of the feature extraction model. Every convolution layer is followed by a pooling layer in the developed model structure.

The fully connected layer is used to integrate the image features extracted by the convolution layer and the pooling layer. Every extracted element is connected to the nodes of the fully connected layer. The proposed model contains three fully connected layers. The activation functions of the first two layers are ReLu, while the last layer adopts softmax as the activation function. The softmax function is usually used for multi-classification [29].

The output of the CNN-based feature extraction model is the senior feature of the input image, i.e. the category of ΔH. Actually, the accuracy of the CNN-based classification is hard to reach 100%, and the wrong extracted senior feature (i.e. the wrong classification result) will lead to the errors in the subsequent regression prediction. Especially for the distinguished categories in the range of $[-10°, 10°]$, the small difference between different categories will easily cause misclassification.

In order to alleviate the influence of the wrong senior feature, a simple and effective method is adopted in this paper. When the vehicle is turning or changing lane, there must be a change of the steering angle. Therefore, the information of the steering angle can be used to judge whether the extracted senior feature is right or wrong. When the extracted senior feature shows that there is a certain angle difference between vehicle direction and road direction, the steering angle within 2s from the current moment is utilized for judgement. If the steering angle does not change, the extracted senior feature is indicated to be wrong and the result is modified to the smallest ΔH category, i.e. senior feature label 8. On the contrary, if the steering angle does change, the result is kept. This method can effectively eliminate the wrong senior features when the vehicle is moving along the road.

B. LS-SVM BASED NONLINEAR REGRESSION MODEL

The changes of the senior feature (the output of the CNN-based feature extraction model) during a period of time is corresponding to the changes of ΔH. Thus, the estimation of ΔH can be achieved by learning the relationship between the changes of senior feature and ΔH.

Support Vector Machine (SVM) is an important traditional Machine Learning algorithm, which uses the expansion theorem of kernel function to establish learning machine in high-dimensional feature space without the explicit expression of nonlinear mapping [30], [31]. After the senior features of the images are extracted, the nonlinear regression model is established by using Least Squares Support Vector Machine (LS-SVM), which has good generalization ability. LS-SVM algorithm replaces the insensitive loss function in SVM with 2-norm error and replaces inequality constraints in SVM with equality ones. Thus, the LS-SVM requires only the solution of a linear equation set instead of the computationally difficult convex quadratic programming problem [32].

Considering a given training set of N_1 data points $\{x_i^{SVM}, y_i^{SVM}\}_{i=1\ldots N_1}$, where $x_i^{SVM} \in \boldsymbol{R}^n$ is the input vector with n dimension, $y_i^{SVM} \in r$ is the output vector with one dimension. In the feature space, the LS-SVM model takes the form:

$$f(x) = \boldsymbol{\omega}^T \varphi(x) + b_s \quad (4)$$

where $\boldsymbol{\omega}$ is an adjustable weight vector; $\varphi(\cdot)$ represents the nonlinear function that maps the input data into higher dimensional feature space; bs is the scalar threshold.

The objective function of LS-SVM is expressed as:

$$\begin{aligned} &\min\ J(\boldsymbol{\omega}, b_s, e_s) = \frac{1}{2}\boldsymbol{\omega}^T\boldsymbol{\omega} + \frac{1}{2}\gamma_s \sum_{i=1}^{N} e_{si}^2 \\ &s.t.\ y_i^{SVM} = \boldsymbol{\omega}^T \varphi(x_i^{SVM}) + b_s + e_{si}, \quad i = 1, \cdots, N_1 \end{aligned} \quad (5)$$

where e_s is the error variable; $\gamma_s \ge 0$ is a regularization constant which can be adjusted and optimized in the training process. Smaller γ_s can avoid the overfitting problem in cases with noisy data.

Using the Lagrange Multiplier Method to rewrite equation (5) into an unconstrained form, the following equation can be obtained:

$$\begin{aligned} L_{SVM} &= \frac{1}{2}\boldsymbol{\omega}^T\boldsymbol{\omega} + \frac{1}{2}\gamma_s \sum_{i=1}^{N} e_{si}^2 \\ &\quad - \sum_{i=1}^{N} \alpha_i^{SVM} \left\{ \boldsymbol{\omega}^T \varphi(x_i^{SVM}) + b_s + e_{si} - y_i^{SVM} \right\} \end{aligned} \quad (6)$$

where $\alpha_i^{SVM} \in r\ (i = 1, \ldots, N_1)$ are the Lagrange multipliers.

Let the partial derivative of equation (6) to $\boldsymbol{\omega}$, b_s, e_s, α_i^{SVM} to be zero:

$$\begin{cases} \dfrac{\partial L_{SVM}}{\partial \boldsymbol{\omega}} = 0 \rightarrow \boldsymbol{\omega} = \sum_{i=1}^{N} \alpha_i^{SVM} \varphi(x_i^{SVM}) \\ \dfrac{\partial L_{SVM}}{\partial b_s} = 0 \rightarrow \sum_{i=1}^{N} \alpha_i^{SVM} = 0 \\ \dfrac{\partial L_{SVM}}{\partial e_k} = 0 \rightarrow \alpha_i^{SVM} = \gamma_s e_{si}, \quad i = 1, \cdots, N_1 \\ \dfrac{\partial L_{SVM}}{\partial \alpha_i^{SVM}} = 0 \rightarrow \boldsymbol{\omega}^T \varphi(x_k^{SVM}) \\ + b_s + e_{si} - y_i^{SVM} = 0, \quad i = 1, \cdots, N_1 \end{cases} \tag{7}$$

Using the equation set of (7) to eliminate $\boldsymbol{\omega}$ and e_{si} can yield a linear system and avoid the quadratic programming problem:

$$\begin{bmatrix} 0 & \mathbf{1}_N^T \\ \mathbf{1}_N & \boldsymbol{\Omega} + \boldsymbol{I}_N/\gamma_s \end{bmatrix} \begin{bmatrix} b_s \\ \boldsymbol{\alpha}^{SVM} \end{bmatrix} = \begin{bmatrix} 0 \\ \boldsymbol{Y}^{SVM} \end{bmatrix} \tag{8}$$

where $\boldsymbol{Y}^{SVM} = [y_1^{SVM}, \cdots, y_N^{SVM}]^T$; $\mathbf{1}_N$ is a n dimension vector with all the elements set as 1; $\boldsymbol{\alpha}^{SVM} = [\alpha_1^{SVM}, \cdots, \alpha_N^{SVM}]^T$; $\boldsymbol{I}_N$ is a $N \times N$ identity matrix; $\boldsymbol{\Omega} \in \boldsymbol{R}^{N \times N}$ is the kernel matrix defined by

$$\Omega_{ij} = \varphi(x_i^{SVM})^T \varphi(x_j^{SVM}) = K(x_i^{SVM}, x_j^{SVM}) i, j = 1, \cdots, N_1 \tag{9}$$

where $K(\cdot, \cdot)$ is the kernel function.

In this model, the radial basis function (RBF) is used:

$$K(x, x_i^{SVM}) = \exp\left\{ -\frac{\left\| x - x_i^{SVM} \right\|_2^2}{2\sigma_{RBF}^2} \right\}, \quad i = 1, \cdots, N_1 \tag{10}$$

where $\left\| x - x_i^{SVM} \right\|_2^2$ is the squared Euclidean distance between the two feature vectors; σ_{RBF} represents the variance of RBF, which can be adjusted and optimized in the training process.

Further, the function expression of LS-SVM model for regression can be written as:

$$f(x) = \sum_{i=1}^{N} \alpha_i^{SVM} K(x, x_i^{SVM}) + b_s \tag{11}$$

where α_i^{SVM} and b_s can be solved by equation (8).

The input of the nonlinear regression model is the output of the feature extraction model. In order to take consideration of the time-related characteristics of ΔH, two delay modules are utilized to delay the output of the feature extraction model. The delayed senior feature labels during last two time steps are set as the input together with the current senior feature label:

$$LS - SVM_{input} = \left[\xi(k)\ \xi(k-1)\ \xi(k-2) \right] \tag{12}$$

where ξ is the senior feature label outputted by the CNN based feature extraction mode; k represents the current time step.

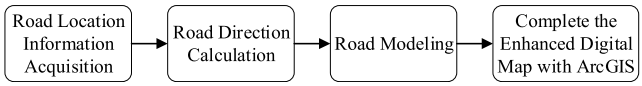

FIGURE 3. The establishing process for the enhanced digital map containing road direction information.

Obviously, the output of LS-SVM model is the angle difference between vehicle driving direction and road direction:

$$LS - SVM_{output} = [\Delta H(k)] \tag{13}$$

After the intelligent perception model of heading-related information is established, the must be well trained before the model can be used to estimate the value of ΔH. In order to achieve good estimation performance, the training samples should contain all categories of senior features in different environments.

IV. ENHANCED DIGITAL MAP CONTAINING ROAD DIRECTION INFORMATION

Compared with traditional digital map, the road direction information is introduced to the enhanced digital map in this paper. When using the enhanced digital map to provide the road direction, the procedure of map matching is executed and the result of map matching is used to determine the output. Thus, the enhanced digital map should have high precision to avoid the matching errors caused by the insufficient accuracy of the map position.

The process to establish the enhanced digital map is shown in Figure 3. The road location with high precision is acquired to ensure the high accuracy of the digital map. Note that, in order to ensure the continuity of road direction information, the data acquisition and production process of each road in the digital map is carried out independently.

The acquired road location points $P_q(\lambda_q, L_q)$ are defined as road nodes, where the subscript q presents the qth location point, λ is the longitude, and L is the latitude. The core of the enhanced digital map in this paper is to calculate the direction of each road node. In order to calculate the direction of the road node, the direction between two adjacent road nodes should be calculated first. Considering that the Gauss plane rectangular coordinate system is usually adopted to display the published map and the direction between two road nodes can be easily calculated in the plane rectangular coordinate, the acquired road position information is transformed from the Earth Centered Earth Fixed coordinate system (longitude and latitude) to the Gauss plane rectangular coordinate system before calculating the direction information. After that, the slope of each road node is calculated to obtain the direction of the road node. Besides, the slope of the road node is also a necessary parameter to establish the road model. In this study, five adjacent road nodes are used to calculate the slope of the intermediate node, which is also known as the AKIMA method [33].

The slope of the line segment between two adjacent nodes can be expressed as:

$$m_q = \frac{Y_{q+1} - Y_q}{X_{q+1} - X_q} q = 1, 2, \ldots, M-1 \tag{14}$$

where X_q is the vertical coordinate of the qth road node in the Gauss plane rectangular coordinate system, Y_q is the horizontal coordinate of the qth road node in the Gauss plane rectangular coordinate system, M is the total number of the road nodes.

According to the AKIMA method, the slope of the qth node can be expressed as:

$$t_q = \begin{cases} \frac{1}{2}(m_{q-1} + m_q) & m_{q-2} = m_{q-1} \neq m_q = m_{q+1} \\ \frac{|m_{q+1} - m_q| \cdot m_{q-1} + |m_{q-1} - m_{q-2}| \cdot m_q}{|m_{q+1} - m_q| + |m_{q-1} - m_{q-2}|} & \text{other} \end{cases}$$
$$q = 1, 2, \ldots, M \tag{15}$$

In order to calculate the slopes of all the road nodes, some equations should be supplemented, including $m_0 = 2m_1$-m_2, $m_{-1} = 2m_0$-m_1, $m_M = 2m_{M-1}$-m_{M-2}, $m_{M+1} = 2m_M$-m_{M-1}.

The direction information of each road node can be obtained by executing the arctangent operation of the results of equation (15). The principal value range of the arctangent function is $[-90°, 90°]$, however the heading angle range in this paper is defined as $[0, 360°]$. Besides, the north direction is defined as 0°, and the heading angle increases in the clockwise direction. The road direction should have the same definition with the heading angle. Thus, the direction of the qth road node in the heading angle range defined above can be expressed as follows:

$$\theta_q = \begin{cases} \frac{\pi}{2} - arctan(t_q), & X_q < X_{q+1} \\ \frac{3}{2}\pi - arctan(t_q), & X_q > X_{q+1} \end{cases} \tag{16}$$

The road direction calculated by equation (16) is determined by the driving direction of the vehicle during the data acquisition process. For two-way roads, they have two opposite road directions. The opposite road direction can be obtained by adding or subtracting π to the direction obtained by equation (16).

Similarly, the AKIMA method is adopted to establish the cubic polynomial curve equation between two adjacent road nodes as the road model. In order to keep the smoothness of the road model, the whole road should have continuous first order derivative. For the interval of two adjacent nodes (X_q, Y_q) and (X_{q+1}, Y_{q+1}), the following equations should be satisfied:

$$\begin{cases} Y_q = f(X_q) \\ Y_{q+1} = f(X_{q+1}) \\ \frac{dY_q}{dX_q} = t_q \\ \frac{dY_{q+1}}{dX_{q+1}} = t_{q+1} \end{cases} \tag{17}$$

Then, the cubic polynomial determined by the interval of $[q, q+1]$ is

$$f(x) = \tau_0 + \tau_1(x - X_q) + \tau_2(x - X_q)^2 + \tau_3(x - X_q)^3 \tag{18}$$

where $\tau_0 = Y_q$, $\tau_1 = t_q$, $\tau_2 = (3m_q - 2t_q - t_{q+1})/(X_{q+1} - X_q)$, $\tau_3 = (t_{q+1} + t_q - 2m_q)/(X_{q+1} - X_q)^2$.

Finally, the road models, the road directions, and the longitude and latitude information of the road nodes are imported into the digital map-making software ArcGIS to complete the enhanced digital map [34].

The process above completes the production of one single road model in the enhanced digital map. When the required enhanced digital map contains multiple roads, the process above should be repeated for every road.

It should be noted that the enhanced digital map only contains the direction information of the road nodes. When using the enhanced digital map, the road direction of any arbitrary point of the road can be obtained through the interpolation method. Besides, another convenient and fast method can be adopted. Considering that the distance between two adjacent road nodes used to establish the enhanced digital map is short, the difference between the direction information of the nearest road node and the actual position is small. Thus, the road direction of the nearest road node captured by map matching can be determined as the output, i.e. the road direction of the actual vehicle position.

V. EXPERIMENTS AND RESULTS

A. EXPERIMENTAL EQUIPMENT AND TRAJECTORIES

In order to verify the feasibility and accuracy of the proposed heading angle estimation methodology, several experiments were conducted by using a Chery TIGGO5 sport utility vehicle on real road. The sensors used in the experiments included a high-precision integrated navigation system SPAN-CPT, a low-cost GPS, and a camera. The positioning accuracy of SPAN-CPT system is 0.01 m with GNSS observations and 0.02 m during 10-s outages. The heading angle accuracy of SPAN-CPT system is 0.03°. In this experiment, the position information collected by the SPAN-CPT system was used to make the enhanced digital map containing road direction information, and the heading angle information was also used as a reference to verify the accuracy of the proposed heading angle estimation methodology. The low-cost GPS adopted the C230-AT provided by Beijing BDStar Navigation Company Ltd. The accuracy for the position is 3 m with available GPS signal. Note that it is the vehicle position that is required for the map matching process of the proposed methodology rather than the GPS. The vehicle position can also be provided by other sensors or methods, such as the Dead-Reckoning method using odometer or INS. In order to obtain the vehicle position information conveniently, the low-cost GPS was used during our experiment. The on-board network camera was provided by the Hikvision. During the experiments, the camera was installed at the middle part of

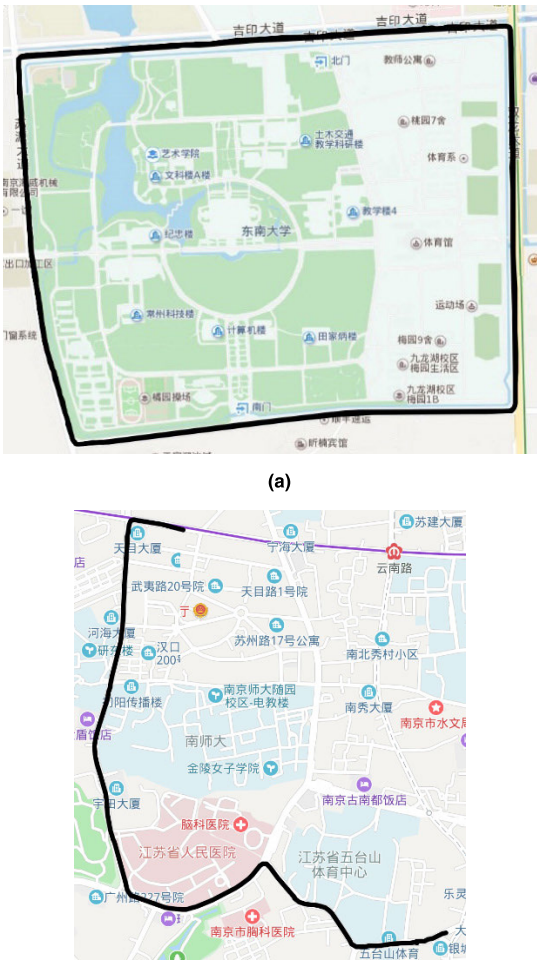

FIGURE 4. The two road-test trajectories of the experiments: (a) trajectory 1; (b) trajectory 2.

the front windshield inside the vehicle to capture the image information in front of the vehicle.

The trajectories during the experiments are shown in Figure 4. Different road types were taken into consideration when choosing the trajectories, including straight, 90° turn, and curve. Besides, some typical urban driving maneuvers, such as lane changing, were conducted during the experiments. The road types and driving maneuvers are conducive to verifying the performance of the proposed intelligent heading angle estimation method.

B. RESULTS OF THE ENHANCED DIGITAL MAP

The enhanced digital maps of the two test trajectories are shown in Figure 5. The red lines represent the road with direction information modeled by the data acquired by the SPAN-CPT system. During the experiments, the shortest projection distance method is adopted for map matching, and the output of the enhanced digital map is the road direction information of the nearest node according to the matching result.

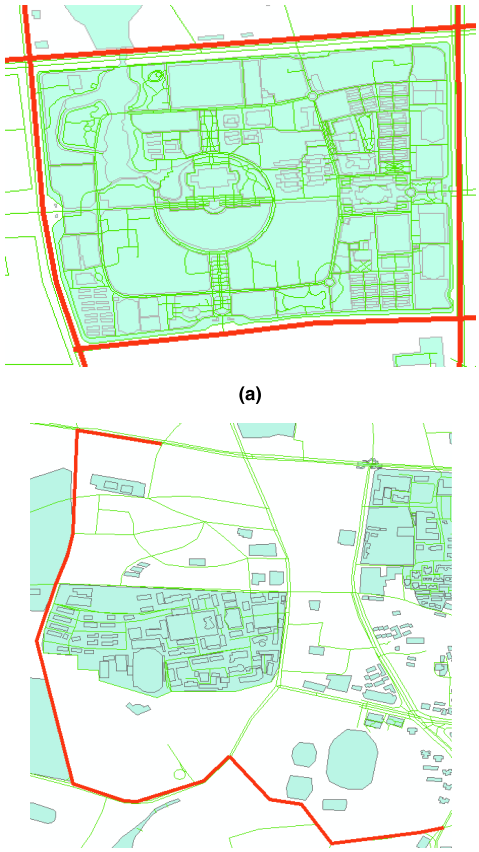

FIGURE 5. The enhanced digital map of the experimental trajectories: (a) the map of trajectory 1; (b) the map of trajectory 2.

C. SAMPLES AND TRAINING PROCEDURE OF THE INTELLIGENT PERCEPTION MODEL

Sample preparation is the prerequisite to train the intelligent perception model of heading-related information. The quantity and quality of the samples determine the application performance of the model.

During the process of making the enhanced digital map mentioned above, the camera information and the vehicle heading information obtained by the SPAN-CPT system are also collected synchronously with the road location information. The true value of ΔH can be calculated by subtracting the road direction provided by the enhanced digital map from the heading angle provided by the SPAN-CPT system. The true ΔH is the target value to train the intelligent perception model. Then, the corresponding label of the true ΔH can be obtained according to Table 1. The label information the target value of the senior feature to train the CNN based feature extraction model.

The image information acquired by the camera and label information constitute the samples of the CNN based feature extraction model, while the label information and the true ΔH constitute the samples of the LS-SVM based nonlinear regression model.

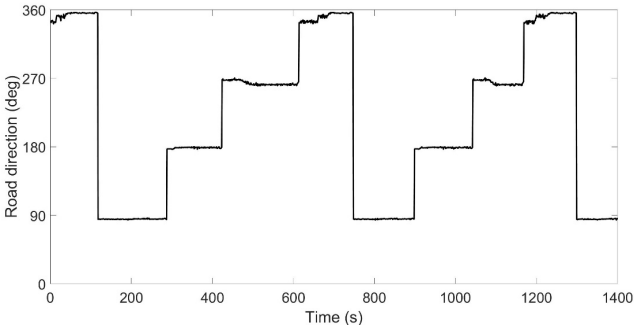

FIGURE 6. The road direction obtained by the enhanced digital map during trajectory 1.

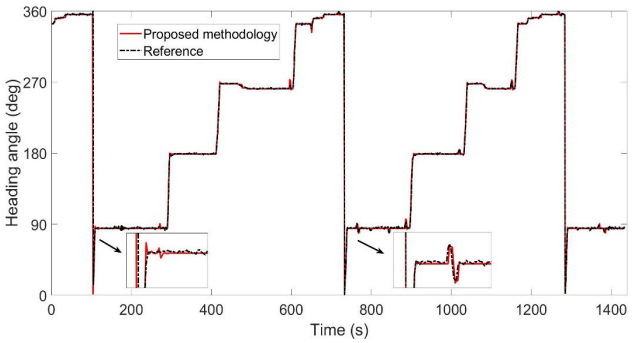

FIGURE 7. The results of the proposed heading angle estimation methodology during trajectory 1.

Note that, when the vehicle is driving along the road, the ΔH is very small. The ΔH can reach relatively high value when the vehicle is turning 90° or changing lane. In order to keep the balance of various senior features in the training samples, the number of the training samples during large maneuvers (90° turn, lane change, etc.) should be close to the number of the training samples during small maneuvers (driving along the road).

After the training examples are ready, the CNN based feature extraction model and the LS-SVM based nonlinear regression model are trained separately.

D. VALIDATION OF HEADING ANGLE ESTIMATION

Utilizing the well-trained intelligent perception model and the established enhanced digital map, the validation of heading angle estimation is conducted by re-acquiring the sensor data on the two trajectories mentioned above.

The road direction obtained by matching the vehicle position with the enhanced digital maps during the experiment on trajectory 1 is shown in Figure 6. It can be seen that output direction is accurate and reliable using the map matching algorithm.

For trajectory 1, the accuracy for senior feature extraction (i.e. the classification accuracy) is 94.7%. Although the accuracy is high, the several wrong senior features will cause estimation error of the heading angle. After correcting the wrong senior feature using the method mentioned at the end of Section III.A, the final estimation results of the heading angle can be obtained, as shown in Figure 7. The reference is the vehicle heading angle provided by the SPAN-CPT. It can be seen that the proposed methodology can accurately estimate the heading angle during the whole experiment, even the vehicle is turning or changing lane. To clearly demonstrate the performance of the proposed positioning methodology, two representative situations were chosen to show the estimation results, as magnified in Figure 7. Figure 8 illustrates the actual scene taken by the camera during the magnified 90° turn process, while Figure 9 gives the scene during the magnified lane changing process.

The output of the enhanced digital map (road direction) during trajectory 2 is shown in Figure 10, while the results

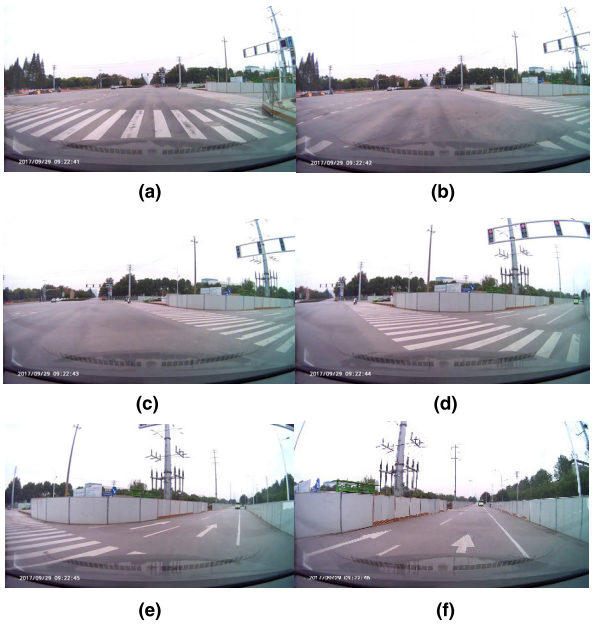

FIGURE 8. The scene of 90° turn during trajectory 1.

of the proposed heading angle estimation methodology on this trajectory are illustrated in Figure 11. During this trajectory, there are more curves than trajectory 1, thus the task of extracting senior feature is more difficult and it is more challenging to estimate the heading angle. From Figure 11, it can be seen that the estimation results of the proposed methodology are close to the reference on the whole.

The statistics of the heading angle errors during the experiments on the two trajectories are shown in Table 2. The errors on trajectory 2 is a little bit larger than those on trajectory 1. There are many straight ways on trajectory 1 and the change of scene is not significant. These are all to the benefit of the estimation results. For trajectory 2, there are more curves and the change of scene is significant. These all raise the difficulty of heading angle estimation. However, the heading angle errors remain small in general. The proposed heading angle estimation methodology can achieve high accuracy on both trajectories.

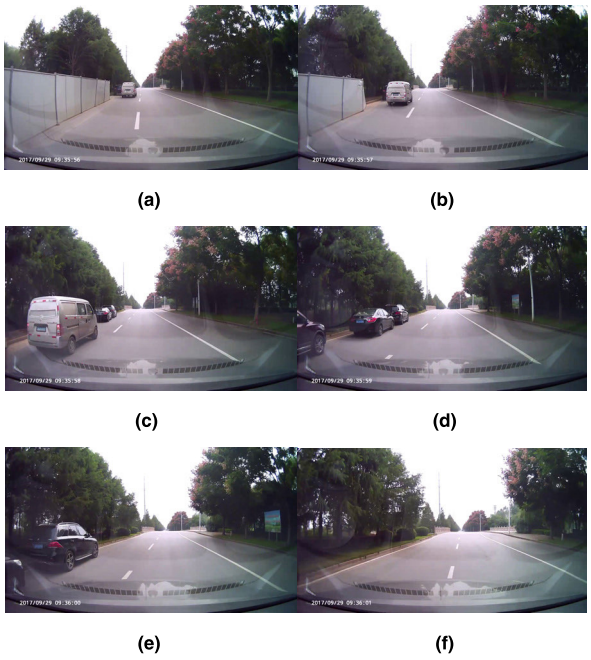

FIGURE 9. The scene of lane change during trajectory 1.

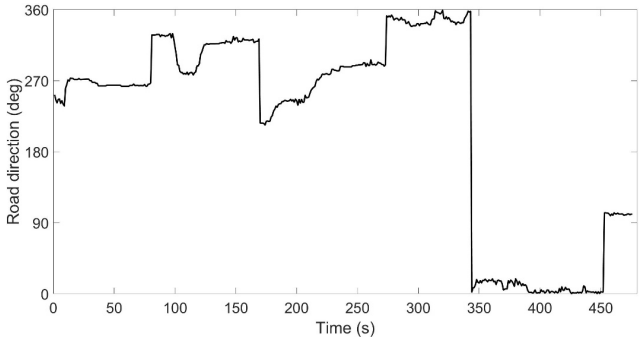

FIGURE 10. The road direction obtained by the enhanced digital map during trajectory 2.

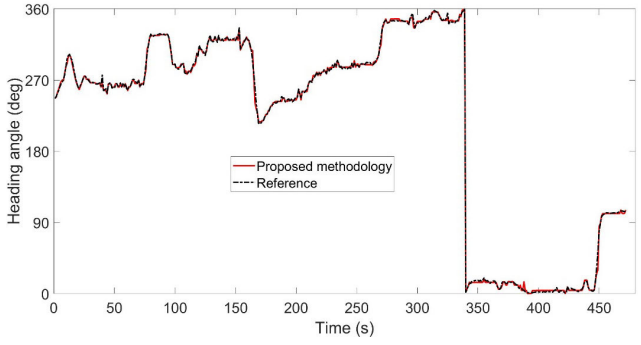

FIGURE 11. The results of the proposed heading angle estimation methodology during trajectory 2.

E. ANALYSIS AND DISCUSSIONS

Due to different hardware, measuring principle, and operating environment, it is difficult to give an accurate and fair comparison between our proposed heading angle estimation methodology and others. We make the following analysis and discussions to further demonstrate the superiority of our proposed methodology.

TABLE 2. Statistics of the heading angle errors during the two trajectories.

	Average error	RMS error
Trajectory 1	0.79°	1.36°
Trajectory 2	1.22°	1.64°

TABLE 3. Comparison between the affordable heading angle estimation methods for land vehicles.

Sensor	Reliability	Disadvantages
MEMS-IMU MEMSIC VG440	Poor	The accuracy will drift with time when GPS signal is blocked.
Digital compass KVH C100	Poor	Compensation is mandatory; easily affected by magnetic interference.

Two typical sensors using different measuring principles are selected to compare with our proposed methodology. One is the MEMS-based IMU MEMSIC VG440, the other is the compass engine KVH C100. These two sensors are usually used to measure the heading angle, and they are both affordable for civil vehicles. The comparison of the reliability and disadvantages are listed in Table 3.

In conclusion, our proposed methodology can achieve equivalent accuracy with the nominal value of the two common sensors mentioned above. The VG440 can reach the accuracy of 1° with valid GPS-Aiding input data, while the KVH C100 has the accuracy of 0.5° after compensation in a free magnetic field. Based on the results shown in Section V.D, the accuracy of the proposed methodology can be determined as $<1.64°$. However, our proposed methodology can essentially avoid the disadvantages of the poor reliability of the two sensors. The heading accuracy of VG440 will rapidly decline when the GPS aiding data is unavailable. The accuracy of KVH C100 will degrade when facing magnetic interference. Thus, we can confirm that the proposed heading angle estimation methodology has certain advantages over the existing methods.

VI. CONCLUSION

This paper has presented a novel heading angle estimation methodology for land vehicles using low-cost sensors. The goal is to propose a heading angle estimation solution that is not affected by the complex urban environment and is immune to cumulative errors.

The proposed methodology combines the advantages of deep learning and enhanced digital map to achieve an accurate and reliable heading angle estimation for land vehicles. First, the proposed methodology employs an intelligent perception model of heading-related information to estimate

the angle difference between the vehicle driving direction and the road direction (ΔH). The intelligent perception model utilizes CNN to extract senior feature, i.e. the label of corresponding ΔH range, and adopts LS-SVM to predict ΔH based on the extracted senior feature. Then, an enhanced digital map is established to provide the road direction through map matching. Finally, the heading angle of the vehicle can be obtained by combining the predicted ΔH and the road direction.

The proposed heading angle estimation methodology is successfully implemented and evaluated through field tests. The experimental results indicate that the proposed methodology can achieve good performance on different road types, including straight, curve, 90° turn, etc. Through analyzing and comparing the proposed methodology with existing representative methods, it can be concluded that our approach fulfills the objective of providing an accurate and low-cost heading angle estimation solution in the urban environment.

REFERENCES

[1] S. Behere and M. Törngren, "A functional reference architecture for autonomous driving," *Inf. Softw. Technol.*, vol. 73, pp. 136–150, May 2016.
[2] S. A. R. Flórez, V. Frémont, P. Bonnifait, and V. Cherfaoui, "Multi-modal object detection and localization for high integrity driving assistance," *Mach. Vis. Appl.*, vol. 25, no. 3, pp. 583–598, 2014.
[3] Y. S. Suh, "Orientation estimation using a quaternion-based indirect Kalman filter with adaptive estimation of external acceleration," *IEEE Trans. Instrum. Meas.*, vol. 59, no. 12, pp. 3296–3305, Dec. 2010.
[4] J.-H. Wang and Y. Gao, "Multi-sensor data fusion for land vehicle attitude estimation using a fuzzy expert system," *Data Sci. J.*, vol. 4, pp. 127–139, Apr. 2005.
[5] Y. Zhang, F. Yu, Y. Wang, and K. Wang, "A robust SINS/VO integrated navigation algorithm based on RHCKF for unmanned ground vehicles," *IEEE Access*, vol. 6, pp. 56828–56838, 2018.
[6] R. Lu, X. Lin, X. Liang, and X. Shen, "A dynamic privacy-preserving key management scheme for location-based services in VANETs," *IEEE Trans. Intell. Transp. Syst.*, vol. 13, no. 1, pp. 127–139, Mar. 2012.
[7] R. Attia, R. Orjuela, and M. Basset, "Combined longitudinal and lateral control for automated vehicle guidance," *Vehicle Syst. Dyn.*, vol. 52, no. 2, pp. 261–279, Jan. 2013.
[8] Y. N. Korkishko, V. A. Fedorov, V. G. Ponomarev, I. V. Morev, S. F. Skripnikov, M. I. Khmelevskaya, A. S. Buravlev, S. M. Kostritskii, I. V. Fedorov, A. I. Zuev, V. K. Varnakov, and V. E. Prilutskii, "Strapdown inertial navigation systems based on fiber-optic gyroscopes," *Gyroscopy Navigat.*, vol. 5, no. 4, pp. 195–204, Oct. 2013.
[9] H. Liu, S. Nassar, and N. El-Sheimy, "Two-filter smoothing for accurate INS/GPS land-vehicle navigation in urban centers," *IEEE Trans. Veh. Technol.*, vol. 59, no. 9, pp. 4256–4267, Nov. 2010.
[10] D. C. Jeronymo, Y. C. C. Borges, and L. dos S. Coelho, "A calibration approach based on Takagi–Sugeno fuzzy inference system for digital electronic compasses," *Expert Syst. Appl.*, vol. 38, no. 11, pp. 13688–13693, Oct. 2011.
[11] Z. Wu, M. Yao, H. Ma, and W. Jia, "Low-cost attitude estimation with MIMU and two-antenna GPS for Satcom-on-the-move," *GPS Solutions*, vol. 17, no. 1, pp. 75–87, 2013.
[12] W. Li and J. Wang, "Effective adaptive Kalman filter for MEMS-IMU/magnetometers integrated attitude and heading reference systems," *J. Navigat.*, vol. 66, no. 1, pp. 99–113, 2013.
[13] X. Gao, Z. Yu, and X. Cheng, "Model based yaw rate estimation of electric vehicle with 4 in-wheel motors," SAE Tech. Paper 2009-01-0463, Jan. 2009.
[14] M. Mirzaei, "A new strategy for minimum usage of external yaw moment in vehicle dynamic control system," *Transp. Res. C, Emerg. Technol.*, vol. 18, no. 2, pp. 213–224, Apr. 2010.
[15] I. F. Mondragón, P. Campoy, M. Olivares, and C. Martinez, "Omnidirectional vision applied to Unmanned Aerial Vehicles (UAVs) attitude and heading estimation," *Robot. Auton. Syst.*, vol. 58, no. 6, pp. 809–819, Jun. 2010.
[16] A. Gil, O. M. Mozos, M. Ballesta, and O. Reinoso, "A comparative evaluation of interest point detectors and local descriptors for visual SLAM," *Mach. Vis. Appl.*, vol. 21, no. 6, pp. 905–920, Oct. 2010.
[17] M. Lee, K. S. Kim, and S. Kim, "Measuring vehicle velocity in real time using modulated motion blur of camera image data," *IEEE Trans. Veh. Technol.*, vol. 66, no. 5, pp. 3659–3673, May 2016.
[18] N. D. Nguyen, T. Nguyen, and S. Nahavandi, "System design perspective for human-level agents using deep reinforcement learning: A survey," *IEEE Access*, vol. 5, pp. 27091–27102, 2017.
[19] Y. Chen, H. Jiang, X. Jia, P. Ghamisi, and C. Li, "Deep feature extraction and classification of hyperspectral images based on convolutional neural networks," *IEEE Trans. Geosci. Remote Sens.*, vol. 54, no. 10, pp. 6232–6251, Oct. 2016.
[20] S. Ohlsson, *Deep Learning: How the Mind Overrides Experience*. New York, NY, USA: Cambridge Univ. Press, 2011.
[21] Y. Hu, J. Gong, Y. Jiang, L. Liu, G. Xiong, and H. Chen, "Hybrid map-based navigation method for unmanned ground vehicle in urban Scenario," *Remote Sens.*, vol. 5, no. 8, pp. 3662–3680, Jul. 2013.
[22] R. Toledo-Moreo, D. Betaille, and F. Peyret, "Lane-level integrity provision for navigation and map matching with GNSS, dead reckoning, and enhanced maps," *IEEE Trans. Intell. Transp. Syst.*, vol. 11, no. 1, pp. 100–112, Mar. 2010.
[23] K. He, X. Zhang, J. Sun, and S. Ren, "Delving deep into rectifiers: Surpassing human-level performance on ImageNet classification," in *Proc. IEEE Int. Conf. Comput. Vis.*, Boston, MA, USA, Dec. 2015, pp. 1026–1034.
[24] L. Jing, M. Zhao, P. Li, and X. Xu, "A convolutional neural network based feature learning and fault diagnosis method for the condition monitoring of gearbox," *Measurement*, vol. 111, pp. 1–10, Dec. 2017.
[25] D. Tran, L. Bourdev, L. Torresani, M. Paluri, and R. Fergus, "Learning spatiotemporal features with 3D convolutional networks," in *Proc. IEEE Int. Conf. Comput. Vis. (ICCV)*, Santiago, Chile, Dec. 2015, pp. 4489–4497.
[26] P. Gysel, M. Motamedi, and S. Ghiasi, "Hardware-oriented approximation of convolutional neural networks," 2016, *arXiv:1604.03168*. [Online]. Available: https://arxiv.org/abs/1604.03168
[27] J. Yang, K. Yu, and T. Huang, "Supervised translation-invariant sparse coding," in *Proc. Comput. Vis. Pattern Recognit. (CVPR)*, San Francisco, CA, USA, Jun. 2010, pp. 3517–3524.
[28] S. Avila, N. Thome, M. Cord, E. Valle, and A. de A. Araújo, "Pooling in image representation: The visual codeword point of view," *Comput. Vis. Image Understand.*, vol. 117, no. 5, pp. 453–465, May 2013.
[29] M. Jiang, Y. Liang, X. Feng, X. Fan, Z. Pei, Y. Xue, and R. Guan, "Text classification based on deep belief network and softmax regression," *Neural Comput. Appl.*, vol. 29, no. 1, pp. 61–70, Jan. 2018.
[30] T. Hacib, Y. L. Bihan, M. R. Mekideche, O. Meyer, L. Pichon, and M. K. Smail, "Microwave characterization using ridge polynomial neural networks and least-square support vector machines," *IEEE Trans. Magn.*, vol. 47, no. 5, pp. 990–993, May 2011.
[31] N. S. Raghavendra and P. C. Deka, "Support vector machine applications in the field of hydrology: A review," *Appl. Soft Comput.*, vol. 19, pp. 372–386, Jun. 2014.
[32] J. Chorowski, J. Wang, and J. M. Zurada, "Review and performance comparison of SVM-and ELM-based classifiers," *Neurocomputing*, vol. 128, pp. 507–516, Mar. 2014.
[33] A. M. Bica, "Optimizing at the end-points the Akima's interpolation method of smooth curve fitting," *Comput. Aided Geometric Design*, vol. 31, no. 5, pp. 245–257, Jun. 2014.
[34] M. Law and A. Collins, *Getting to Know ArcGIS Desktop*. Los Angeles River, CA, USA: ESRI Press, 2010.

QIMIN XU received the B.S., M.S. and Ph.D. degrees in instrument science and technology from Southeast University, Nanjing, China, in 2011, 2014, and 2018, respectively. He is currently a Lecturer with the School of Instrument Science and Engineering, Southeast University. His current research interests include vehicle state estimation, vehicle positioning, and autonomous driving.

XU LI (M'10) received the Ph.D. degree in instrument science and technology from Southeast University, Nanjing, China, in 2006. He is currently a Professor with the School of Instrument Science and Engineering, Southeast University. Since 2002, he has been involved in the research and development of multi-sensor integration navigation, environment perception, and control for automated vehicles. His current research interests include the collaborative perception and control of intelligent vehicle and infrastructure systems, information fusion, automated vehicles, and active safety.

ZHENGLIANG SUN received the B.S. degree from Southeast University, Nanjing, China, in 1987, and the M.S. degree in software engineering from Peking University, Beijing, China, in 2011. He is currently a Research Fellow with the Traffic Management Research Institute, Ministry of Public Security. His current research interests include intelligent transportation systems and traffic information management.

WEIMING HU received the M.S. degree in mechanical engineering and automation from Northeast University, Shenyang, China, in 2017. He is currently pursuing the Ph.D. degree in instrument science and technology with Southeast University, Nanjing, China. His current research interests include prediction of driving maneuver, intelligent driving assessment, and intelligent transportation systems.

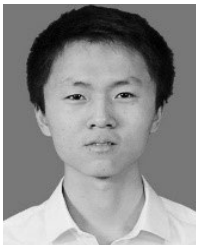

BIN CHANG received the B.S. degree in electrical engineering and automation from Nanjing Tech University, Nanjing, China, in 2018. He is currently pursuing the M.S. degree with the School of Instrument Science and Engineering, Southeast University. His current research interest includes intelligent vehicle perception and positioning.